Applied Nanoscience (2023) 13:3149–3160
https://doi.org/10.1007/s13204-021-01776-w

ORIGINAL ARTICLE

Antioxidant, anticancer and enhanced photocatalytic potentials of gold nanoparticles biosynthesized by common reed leaf extract

Ola M. El-Borady[1] · Manal Fawzy[2,3] · Mohamed Hosny[2]

Received: 11 November 2020 / Accepted: 3 March 2021 / Published online: 19 March 2021

Abstract

This research discloses a single step, facile, cost-effective, and eco-friendly fabrication of gold nanoparticles (AuNPs) using the aqueous extract of common reed (*Phragmites australis*) leaf. Various techniques were employed to characterize the resultant AuNPs such as UV–Vis spectroscopy, high resolution transmission electron microscopy (HRTEM) mapping, fourier transform infrared (FT-IR), Zeta potential, X-ray diffraction (XRD), Energy Dispersive X-ray spectroscopy (EDX), and X-ray Photoelectron Spectroscopy (XPS) to confirm the bioformation of AuNPs. The results showed the formation of violet-colored, mainly spherical shaped AuNPs with about 18 nm diameter. The XRD results proved the crystalline structure of AuNPs. Furthermore, *P. australis*-AuNPs exhibited notable anticancer efficacy with an IC_{50} equals 129 µg/mL, good quenching for DPPH free radical with a scavenging percentage equals 10.26% and a superior photocatalytic activity as they completely removed methylene blue in just 1 min. The current study also provides an open option for the environmental management of the unwanted biomass of common reed.

Keywords Phytosynthesis · Gold nanoparticles · *Phragmites australis* · Cytotoxicity · Antioxidant

Introduction

The study of nanoparticles (NPs) represents a breakthrough in material science from the fundamental point of view and for numerous applications, such as materials reinforcement, as a doping agent for materials conductivity, for drug delivery purposes, or even for cancer cell detection (Neouze 2013).

The scientific and technological significance of metallic NPs has made them the focal point of extensive research, given their unusual chemical and physical characters. Especially, AuNPs which are harnessed in a lot of different areas such as, biosensing, catalysis, electronics and cancer therapy (Geetha et al. 2013; Princy and Gopinath 2018; Thangamani and Bhuvaneshwari 2019).

Various chemical (Sun and Xia 2002; Mhamane et al. 2011; Sedki et al. 2015) and physical (Mafuné et al. 2002) methods were used to synthesize NPs. However, these methods are costly, energy-consuming, and detrimental to the environment. Therefore, biosynthetic approaches, specifically those using plants extracts, arose as a cheaper and safer rout to synthesize nanomaterials. Researchers previously used tea, coffee (Nadagouda and Varma 2008), and other plant extracts since these extracts contain various biological compounds that could act as reducing and stabilizing agent at the same time (Dubey et al. 2010; Narayanan and Park 2015).

Numerous demerits of conventional physical and chemical procedures harnessed for the synthesis of AuNPs were recognized. For instance, the high cost, toxicity issues on human health and the environment in addition to the unselectively apoptosis of healthy cells by the chemically synthesized AuNPs in medical applications as anticancer studies. To counter the aforesaid downsides the move to green-synthesized AuNPs is desirable, as pointed out by Arvindganth and Kathiravan (2019).

✉ Ola M. El-Borady
olachem_elborady@yahoo.com

[1] Kafrelsheikh University, Institute of Nanoscience and Nanotechnology, Kafrelsheikh, Egypt

[2] Green Technology Group, Environmental Sciences Department, Faculty of Science, Alexandria University, Alexandria 21511, Egypt

[3] National Egyptian Biotechnology Experts Network, National Egyptian Academy for Scientific Research and Technology, Cairo, Egypt

Although the history of noble metal NPs dates back to the days of Faraday's groundbreaking work, they are still profoundly researched in up-to-date research (Capek 2017). It was reported that among the numerous forms of metal NPs, AuNPs have a considerable number of applications such as DNA recognition, heredity medicine, and nano-catalysis (Geetha et al. 2013).

It is paramount to state that AuNPs have a plethora of special and unique physicochemical characteristics, including safety, biocompatibility, biodegradability, good fluorescence imaging, high electrical conductivity. Additionally, the surface plasmon resonance (SPR) is the dominating optical feature of AuNPs with a size of 2–100 nm and confers the characteristic bright red color to the colloidal solution of spherical AuNPs. Additionally, AuNPs with a size above about 2 nm have larger extinction cross-sections, with a potentiality of providing 100% of light-to-heat conversion efficiency, high photostability, and the capability to amplify the electromagnetic field near the metal surface. Another property is the onset of quantized (single electron) charging with the NPs behaving as nanoscale molecular capacitors. The chemical properties of AuNPs, such as their catalytic effect, are further highly dependent on their size and shape, as mentioned by Amendola et al. (2014), in addition to surface functionality that enables amines, thiols, and nucleic acids to conjugate with AuNPs by electrostatic interactions (Liu et al. 2016).

With the improvement of nanotechnology in the biological and medical fields, the demand to incorporate NPs into biomolecules, to produce conjugated or hybrid systems increased. This is due to such systems; specifically, AuNPs, are useful in many medical applications (Mohamed et al. 2012). These applications include drug delivery, cancer, and gene therapy, biomolecular detection, imaging, tissue engineering, sensing, theranostics, pharmaceutical products and manipulating the structure of biomolecules, as stated by Torabi et al. (2019).

One of the most important and common tests for the antioxidants against free radicals, is the DPPH. Whereas, the free radicals are harmful and can cause damage to human cells. A substantial role against these free radicals is mainly played by antioxidants such as AuNPs (Markus et al. 2017).

Common reed (*Phragmites australis*) is a perennial, widely distributed emergent macrophyte. It has a vigorous growth and remarkably high amplitude of tolerance, which makes it the dominant plant species in many water courses and often forms huge reed-beds along many shallow lakes and freshwater canals, especially in Egypt (Shaltout et al. 2006).

Phytochemical screening of *P. australis* revealed the presence of glycosides, tannins, phenolic compounds, flavonoids, and terpenoids in the extract of the vegetative parts (Derouiche et al. 2017). Also, the antibacterial and antioxidant potentials of this species was previously reported (Al-Akeel et al. 2010).

In consistent with the transformation to green and sustainable approaches for the synthesis of nanomaterial, here we have explored a contribution for synthesis of AuNPs using the aqueous extract of *P. australis*. The cosmopolitan distribution of common reed, and its availability throughout the year as well as its phytochemicals make it a good candidate for this protocol. The cytotoxicity, antioxidant and photocatalytic potentiality of the phytosynthesized NPs were investigated for possible use in Nano-based applications.

Experimental

Chemicals and reagents

Gold tetrachloroaurate solution ($HAuCl_4.3H_2O$), 2,2-diphenyl-1-picrylhydrazyl (DPPH) (99%), ascorbic acid, and methylene blue (MB) were purchased from Merck, USA. Dimethyl sulphoxide (DMSO) was purchased from HiMedia (India), and A549 cancer cell line was purchased from Vacsera center, Giza, Egypt.

All reagents utilized in this research were of analytical grade, used without further purification. All aqueous solutions were prepared using double-distilled water.

Preparation of plant extract

Common reed leaves were collected from Mariout Lake in northern Egypt, rinsed with deionized water several times to get rid of debris and impurities. Then, fragmented and were left to dry in the open air followed by oven drying overnight at 60 °C. Afterward, dry leaves were ground in a stainless steel mixer to get a fine powder. Five grams from the resultant powder were dissolved in 100 ml deionized water; and the mixture was heated and stirred at 400 rpm using a magnetic stirrer until boiling for 20 min. Finally, the hot solution was filtered. The filtrate extract (pH 5.47) was kept at 4.0 °C for further use.

Biosynthesis of AuNPs

Briefly, 10 mL of the prepared leaf extract was added to 1 mL of $HAuCl_4.3H_2O$ (0.0011 M). The solution mixture was heated until a color transformation was observed from golden yellow to violet. Then the formed colloidal solution was left to cool down and stored at room temperature.

Characterization techniques

The morphological analysis and size distribution of the bioformed AuNPs were detected by HRTEM measurements

performed on a JOEL, JEM-2100F, Japan, accelerating voltage of 200 kV. The bio-reduction of the gold ions to AuNPs was monitored by measuring the UV–Vis spectroscopy measurements on a double-beam spectrophotometer (Shimadzu, Model No-UV 1800), in the scanning range 300–800 nm. Furthermore, the FT-IR spectrum was conducted to assess the possible involvement of functional groups in the leaves extract that liable for the reduction and stabilization process; the measurements were conducted for a ground sample with KBr on a JASCO spectrometer over the range 4000–400 cm^{-1}. The Zeta potential was examined with a zeta potential analyzer (Zetasizer Nano ZS Malvern) to measure the surface charge of AuNPs and their stability while the distilled water was utilized as a diluent. The XRD measurements of lyophilized powder AuNPs were done on an X-ray diffractometer (PXRD-6000 SHIMADZU) operated at a voltage of (40 KV) and current of (30 mA) with CuKa1 radiation ($k = 1.54056A^{o}$) in the angle range of 10–80 °C. The crystallite domain size was calculated from the width of the XRD peaks using the Scherrer formula as given by:

$$(D) = \frac{0.9\lambda}{\beta \cos\theta} \quad (1)$$

where D is average crystallite size, β indicates the line broadening value of the full width at half maximum (FWHM) of the peak, λ is the wavelength of irradiated X-rays, and θ is the maximum peak position value. The elemental conformation investigation was conducted by the energy-dispersive X-ray spectroscopy (EDX) on scanning electron microscope, JEOL model JSM-IT100. XPS was collected on K-ALPHA (Themo Fisher Scientific, USA) with monochromatic X-ray Al K-alpha radiation -10 to 1350 eV spot size 400 micro m at pressure 10–9 mbar with full-spectrum pass energy 200 eV and at narrow-spectrum 50 eV. The powder sample was pressed onto a sample holder, which was placed in a vacuum chamber. The pressure in the analysis chamber was below 10–9 mbar during the analysis. The binding energy (BE) was determined utilizing *C* 1 s spectrum as a reference at 284.58 eV.

Estimation of cell viability—MTT assay

The MTT assay is a colorimetric assay for measuring cellular enzymes' activity that reduces the tetrazolium dye, MTT, to its insoluble formazan, giving a purple color. This assay was carried out to test the ability of the synthesized AuNPs to inhibit the growth and proliferation of human lung cancer cell line (A549) and to determine the IC_{50}, which is the concentration required to kill 50% of cancerous cells by the biosynthesized AuNPs. A549 lung cancer cell line was purchased from Vacsera, Giza, Egypt and it was cultured in Dulbecco's Modified Eagles medium (Gibco-BRL, Grand Island, NY, USA) supplemented with 10% fetal bovine serum and 1% penicillin/streptomycin (Gibco-BRL, Grand Island, NY, USA) at 37 °C in a humidified atmosphere containing 5% CO_2 and 95% air. The cytotoxicity of AuNPs synthesized by P. australis against A549 cancer cells were examined using 3-(4,5-dimethyl-2-thiazolyl)— 2,5-diphenyl-2H tetrazolium bromide (MTT) (Life Technologies, Eugene, Oregon, USA) assay. Cells were seeded at a density of 1×10^4 per well in a 96-well plate (Corning Costar, Lowell, NY, USA) and then treated with different concentrations of AuNPs synthesized by P. australis (0.097–200 µg/mL) at 37 °C at 90% confluency. After 2 days of incubation, 50 µL of MTT assay solution (5 mg/mL phosphate buffer saline) was added to each well and further incubated at 37 °C for 4 h. Then, 50 µL of dimethyl sulfoxide was added to dissolve the formazan crystals. Finally, each well's absorbance was measured at 570 nm using an enzyme-linked immunosorbent assay reader (Bio-Tek Instruments, Inc., Vinooski, VT, USA) (Manivasagan et al. 2015; Nakkala et al. 2015; Parveen and Rao 2015; Abel et al. 2016). The optical density of formazan formed in untreated cells (negative control) represents 100% cell viability. All the experiments were triplicated; mean and standard deviations were calculated.

The percentage of cell viability was calculated by the following Eq. (2).

$$\text{Percentage of viability} = \frac{(\text{OD value of experimental sample})}{\text{OD value of experimental control}} \times 100 \quad (2)$$

where OD stands for optical density.

Antioxidant activity (DPPH assay)

DPPH is a stable and harmful free radical that could be scavenged upon accepting electron or hydrogen from AuNPs (Ramamurthy et al. 2013). The free radical scavenging activity was examined via DPPH (2, 2-diphenyl-1-picrylhydrazyl) assay to determine the antioxidant activity of the AuNPs. In the process, one mL of root and rhizome synthesized-AuNPs were mixed (each one separately) with one mL of DPPH (0.2 mM). A control DPPH assay was conducted without AuNPs. The assay was conducted in triplicates. These mixtures were kept in the dark condition for 3 min at ambient temperature. After 20 min, the developed concentration of radical is examined by the reduction in absorbance percentage of the mixture at 517 nm. Ascorbic acid was utilized as a reference and the scavenging activity was calculated by the following equation:

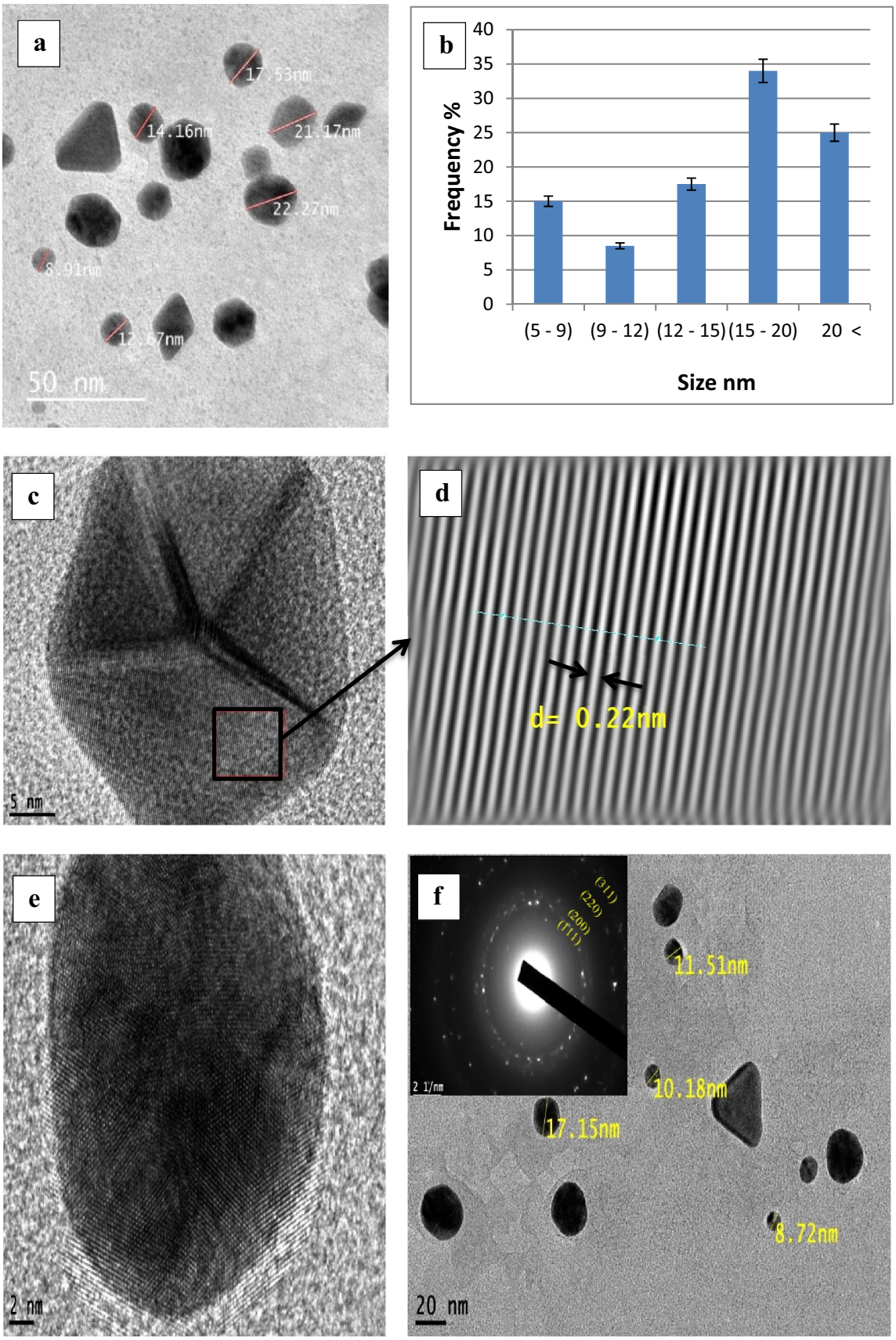
a
17.53nm
14.16nm
21.17nm
22.27nm
8.91nm
12.67nm
50 nm
b
Frequency %
40
35
30
25
20
15
10
5
0
(5 - 9)
(9 - 12)
(12 - 15)
(15 - 20)
20 <
Size nm
c
5 nm
d
d= 0.22nm
e
2 nm
f
(311)
(220)
(200)
(111)
2 1/nm
11.51nm
10.18nm
17.15nm
8.72nm
20 nm

◂**Fig. 1** **a** TEM image of AuNPs **b** Size distribution histogram of the phytosynthesized AuNPs **c** HRTEM image of AuNPs **d** The interplanes spacing $d = 0.22$ nm **e** HRTEM image of AuNPs **f** TEM image of AuNPs (inset) selected area electron diffraction image (SAED) of AuNPs

$$\text{Radical scavenging activity} = \frac{(\text{Control absorbance} - \text{sample absorbance}) \times 100}{\text{control absorbance}} \quad (3)$$

Where control absorbance is the absorbance in the absence of antioxidants and sample absorbance is the absorbance in the presence of antioxidants (AuNPs or Vitamin C) at 517 nm.

Photocatalytic potential

The photocatalytic potential of green synthesized AuNPs is defined as its ability to remove toxic pollutants such as methylene blue (MB) dye by the aid of Ultra Violet (UV) light irradiation as indicated in various research works such as Vijayan et al. (2019). The larger surface area of nanomaterials, the greater the catalytic activity (Ganapuram et al. 2015), and this is what renders AuNPs to be a prominent candidate for removing toxic dyes including MB.

Photocatalytic activity of AuNPs against MB dye was conducted in the presence of UV light. The experiment was conducted with two different AuNPs volumes, 250 and 500 µL, with a concentration of 200 µg/mL. In each experiment, AuNPs was mixed with 2.5 mL of 5×10^{-5} M (MB) and stirred for 30 min in dark condition for adsorption–desorption equilibrium then the solutions were exposed to UV light. Furthermore, control experiments were conducted with the same conditions but in the absence of AuNPs.

The degradation effect was recorded by measuring the UV–Vis spectra of all solutions, and the removal efficiency was calculated by Eq. (4).

$$\text{Percentage of removal (\%) of MB} = \frac{\text{A0} - A}{\text{A0}} \times 100 \quad (4)$$

Where (A_o) refers to the initial absorbance, and (A) refers to the final absorbance.

Results and discussion

HRTEM imaging and SAED techniques

Transmission electron microscopy (TEM) is considered quintessential in delivering necessary information such as the shape and the size of NPs (Lee et al. 2019).

Transmission electron microscopy images of the bioformed AuNPs using the leaves extract are represented in Fig. 1a, f and size distribution is shown in Fig. 1b. The images indicated that the spherical shape was the dominant with a size diameter around 18 nm. However, triangle, hexagonal and rhomboid shapes were also present with low incidence. Similar shapes were also recorded by Manikandakrishnan et al. (2019) who stated that multi-shaped or uneven shape of the green synthesized AuNPs is mainly attributed to the presence of different phytoconstituents in plant extracts. The appearance of NPs in completely discrete form, unraveling that the common reed leaves extract, could efficiently protect AuNPs from aggregation.

The crystallographic structure of AuNPs was deduced from high-resolution transmission electron microscopy (HRTEM) images as shown in Fig. 1c, e, the AuNPs are of crystalline structure consisting of several crystalline lattices with well-defined inter-planer spacing $d = 0.22$ nm, which is shown in Fig. 1d. Additionally, the crystalline structure of the phytosynthesized AuNPs was confirmed by utilizing the selected area electron diffraction (SAED) technique demonstrated in inset Fig. 1f, and matched with the XRD results. Moreover, the current results were similar to those obtained by Abdel Hamid et al. (2013), Sett et al. (2016) and Tahar et al. (2019).

Energy dispersive X-ray spectroscopy (EDX) attached to TEM

The EDX was utilized to characterize the elemental compositions of synthesized NPs. In the current analysis, the atoms on the AuNPs were excited by a specific wavelength electron beam. These in turn, emit X-rays at an energy that is element-specific (Sree Satya Bharati et al. 2018). As shown in Fig. 2b, the green EDX mapping revealed that the nanoparticles presented in Fig. 2a are composed of gold since the green color is centered on the NPs. Also, the same result was obtained by Wang et al. (2016) and Tahar et al. (2019). Furthermore, the red EDX mapping, as illustrated in Fig. 2d, indicated that the oxygen was equally distributed all over the map. Therefore, confirming that the NPs are zero-valent state of gold (Au^0), not gold oxide (Au_2O_3) nanoparticles. Moreover, the white color in Fig. 2c represented the carbon that was equally distributed all over the map. Thus, ensuring that the oxygen and carbon were resulting from the phytoconstituents of the plant extract. In other words, they were of plant origin.

Uv–vis spectroscopy

One of the most characteristic features of metallic NPs is the surface plasmon resonance (SPR) band in their absorption spectrum (Noruzi et al. 2012). Furthermore, the color change of the aqueous colloidal solution during heating could be mainly accredited to the excitation

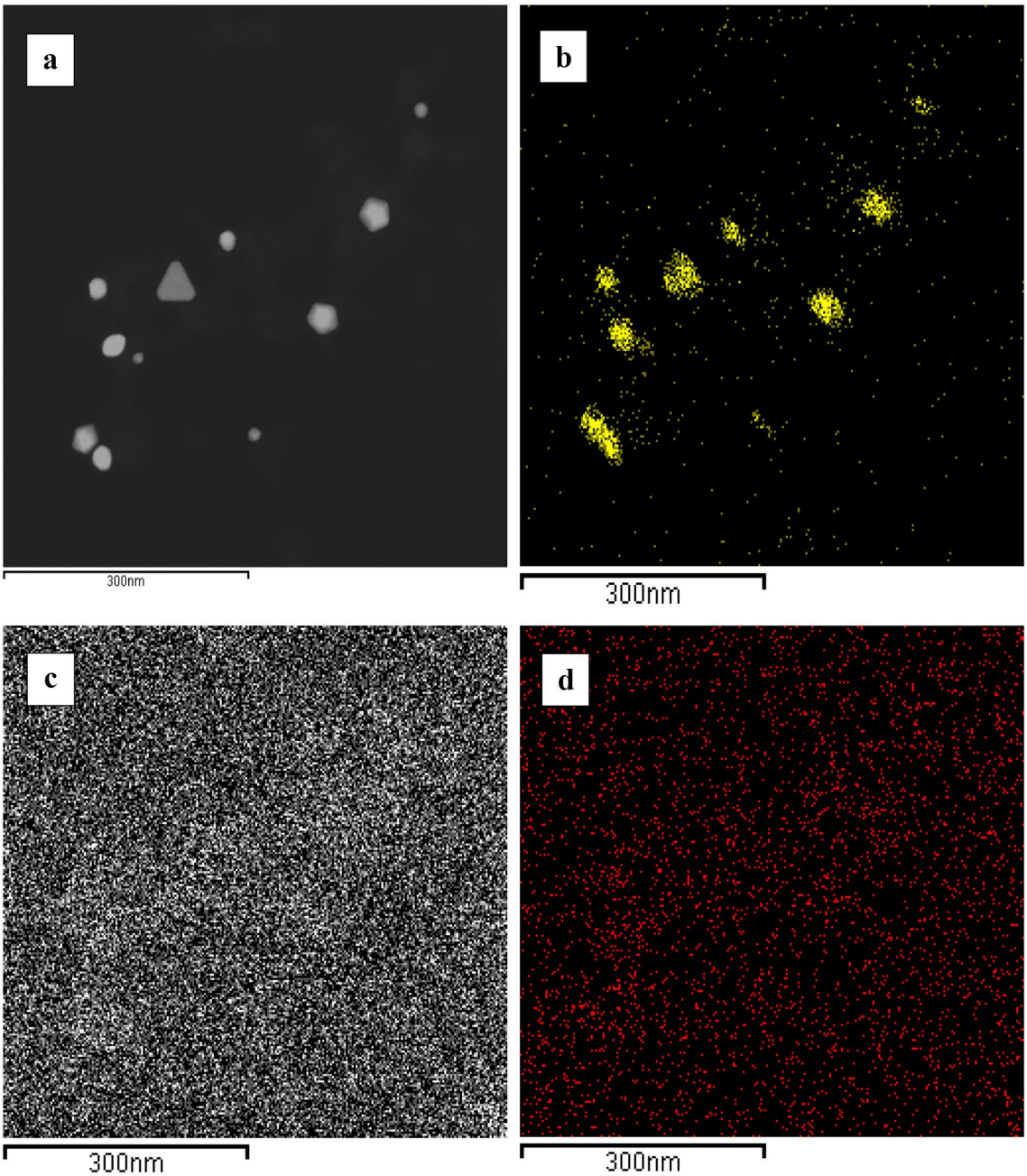

Fig. 2 The elemental mapping analysis of AuNPs using energy dispersive X-ray spectroscopy (EDX) **a** elemental mapping: electron micrograph region of gold nanoparticles **b** distribution of gold element (green) **c** distribution of carbon element (white) **d** distribution of oxygen element (red)

of SPR (Mahendran and Ponnuchamy 2018), while the shape and position of the NPs SPR peak depend on the morphology of NPs (El-Borady et al. 2020). In the current research, AuNPs exhibited a dark violet color (inset Fig. 3b), and its absorption spectrum was seen in Fig. 3b. The absorption chart provided a sharp SPR peak at 540 nm; the peak's sharpness indicates the homogeneity of the phytosynthesized NPs, which was also evidenced by the TEM images. The obtained results were similar to

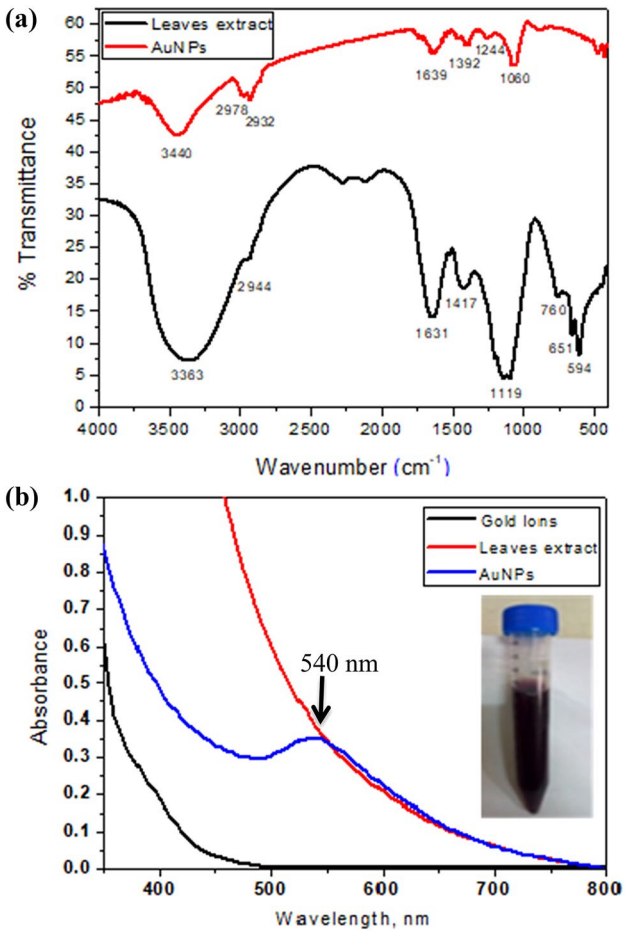

Fig. 3 **a** FT-IR spectra of leaves extract and AuNPs. **b** UV–vis spectra of gold ions, leaves extract and AuNPs; inset, photo for the violet-colored phytosynthesized AuNPs

those obtained recently for AuNPs prepared by the *Cocos nucifera* Linn extract (Paul et al. 2014).

Fourier transform infrared spectroscopy (FT-IR)

Fourier transform infrared spectroscopy is commonly utilized to detect the functional groups, likely contributing to the reduction and the capping of bioprepared nanomaterials (Ganapuram et al. 2015; Narayanan and Park 2015). Figure 3a showed the FTIR spectra for common reed leaves extract compared to AuNPs. In the FT-IR spectrum of the leaves extract, multiple bands were distinguished; peak at 3363 cm^{-1} corresponded (OH) group that shifted to higher wavenumber 3440 cm^{-1} and lower intensity in the spectrum of the AuNPs, 2944 cm^{-1} attributed to C–H (sp^3), 1631 cm^{-1} corresponded to C = C, C–O or C = N bond that slightly shifted to 1639 and lower intensity in the biosynthesized AuNPs. The peak at 1080 in plant extract (C–N stretch vibration of aliphatic amines) shifted to 1119 cm^{-1} in the AuNPs spectrum.

The presence of functional groups like C–N, C–O, O–H, and N–H and shifting its position suggests the presence of some moieties such as proteins, alkaloids, flavonoids, amino acids, and pigments in the plant extract. Consequently, it was deduced that glycosides and flavonoids were liable for the reduction and capping of AuNPs (the mechanism is presented in Fig. 4). Previously, Reddy et al. (2015), synthesized AuNPs from the gum kondagogu extract. Suggesting the binding of AuNPs to hydroxyl group and confirming that the biocompounds containing this functional group such as flavonoids were the main reducing and stabilizing to AuNPs. Additionally, a similar mechanism for the biological synthesis of AuNPs by the extract of *Lawsoniainermis* was proposed by Kumari and Meena (2020) indicated that

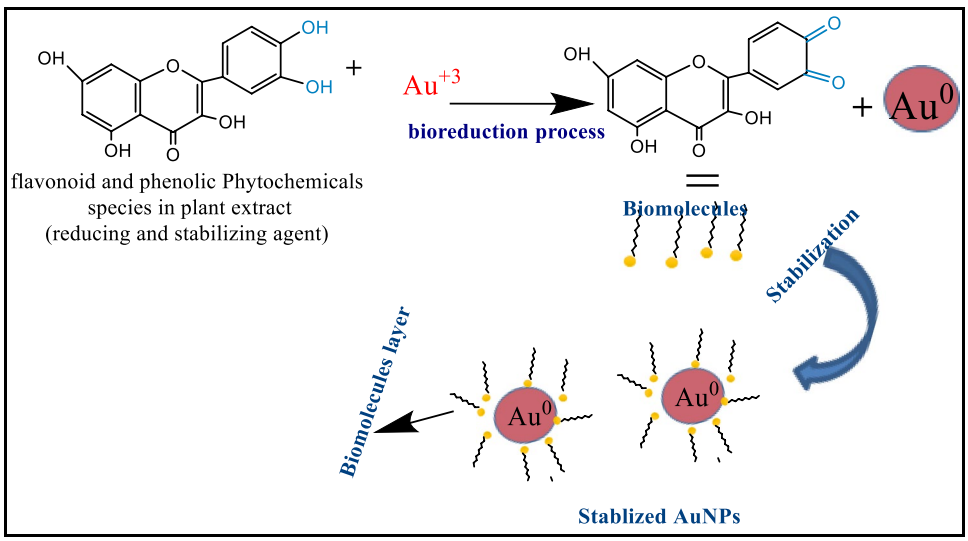

Fig. 4 the suggested mechanism for the reduction process and stabilization of AuNPs by the plant extract

flavonoids were responsible for the reduction and capping of AuNPs.

Zeta potential study

The average zeta potential value of AuNPs was − 13 mV (Fig. 1 supplemental information). This negative value suggested a proper capping of AuNPs due to polyphenolic compounds. The detected value was comparable to that obtained for AuNPs biosynthesized by *Cassia tora* leaves extract (− 12.5 mV) (Abel et al. 2016).

The existence of a negative charge on the surface of AuNPs is commonly attributed to the presence of stabilizing or capping agents formed during the formation and growth of AuNPs, and the negative zeta potential is considered an indicator for the stability of colloidal AuNPs solutions (Chellapandian et al. 2019). As suggested previously (Milaneze et al. 2016), NPs with a zeta potential more than (+ 25 mV) or lower than (− 25 mV) have sufficient electrostatic repulsion to maintain their stability in the solution.

The suggested green synthesis mechanism indicated that the gold metal ions were reduced and further stabilized by the phytoconstituents of *P. australis* such as phenolic compounds and flavonoids. In other words, the phytoconstituents of *P. australis* paly a dual role as reducing and stabilizing agent. Additionally, the current mechanism is similar to numerous previous results, such as the one illustrated by Karmous et al. (2019).

X-ray diffraction (XRD)

The XRD analysis was conducted to define the structure of synthesized AuNPs and their crystallinity (Hamelian et al. 2018a). The results of XRD ensured the face-centered cubic (FCC) structure of the synthesized AuNPs (Fig. 2 supplemental information). The XRD pattern showed peaks detected at 37.63°, 44.16°, 64.25° and 77.36° that was attributed to (111), (200), (220), and (311) planes.

The crystallite size of AuNPs was also calculated using the Scherrer equation and found to be 8.5 nm that is close to the size obtained from TEM image measurements.

Energy dispersive X-ray spectroscopy (EDX) attached to SEM

The EDX analysis is an elemental analytical technique utilized to confirm the existence of elemental gold in the biosynthesized AuNPs (Fig. 3 supplemental information). The EDX chart obtained showed several identified peaks at different emission energies corresponding to the Au metal. Furthermore, other several peaks attributed to carbon, sulpher, oxygen, potassium, cupper elements, and other minerals were recorded due to plant biomolecules that surround or bonded to the surface of AuNPs resulting in the stabilization of biosynthesized AuNPs (Paul et al. 2014; Hamelian et al. 2018b).

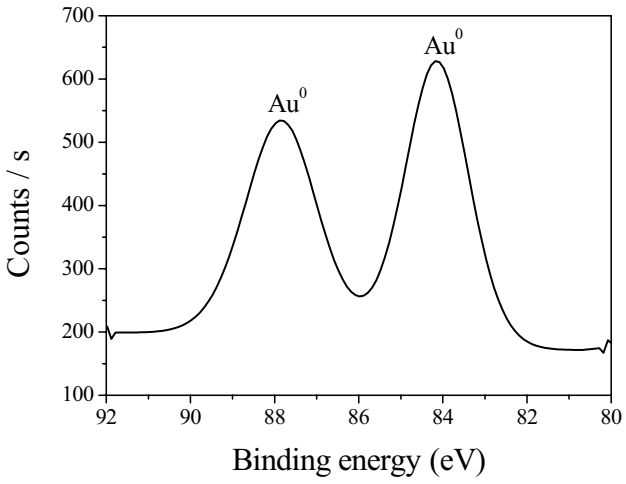

Fig. 5 Experimental XPS spectrum performed on the phytosynthesized AuNPs

X-ray photoelectron spectroscopy (XPS) study

In the current study, XPS was used to analyze the oxidation state of the phytosynthesized AuNPs. The recorded Au 4f spectra were characteristic of metallic Au with Au $4f_{7/2}$ and Au $4f_{5/2}$ binding energies of 84.14 and 87.83 eV, (Fig. 5), respectively, which were concomitant with the previous results (Torres et al. 2002; Ono and Roldan Cuenya 2008; Mikhlin et al. 2010; He et al. 2014). Therefore, confirming that the gold in the phytosynthesized AuNPs was metallic Au^0 (only zero form is formed), not Au_2O_3.

The obtained XPS results confirm the role of phytoconstituents present in *P. australis* extract as an effective reducing agent through the facile reduction of gold species to its zero-valent state, which is the most stable state for gold, as previously mentioned by Rajab et al. (2014).

Estimation of cell viability—MTT assay

In the current study, the anticancer effect of bioprepared AuNPs was tested against cancerous human lung cell line A549 using MTT assay.

Regarding the role played by the phytosynthesized AuNPs in the anticancer method, they have interacted with the biological component of A549 cancer cells in numerous ways. Including alteration of cell membrane integrity, disruption of metabolic and physiological systems, oxidation of functional biomolecules, oxidative stress, ROS production, disturbance of nutrient uptake, inhibition of respiratory chain, disruption of ATP synthesis, and obstruction in the

transfer of electrons, which will lead to shrinkage of cells, cell cycle arrest, and loss of functions in addition to induction of Hyperthermia. Eventually, all these interactions will result in cancer cell death (Apoptosis) as it was clarified by Karmous et al. (2019).

The obtained cytotoxicity results revealed the IC_{50}; the concentration of AuNPs needed for 50% cell death was 129.42 µg/mL. The anticancer effect could be attributed to the penetration of AuNPs into the cell membrane, and interaction with the nucleic acids, proteins and other biomolecules, inhibiting the progression of cancerous lung cells. The % cell viability, which refers to the healthy cells that were persistent to the influence of AuNPs and remained intact after treatment with AuNPs, decreased with increasing concentration of the biosynthesized AuNPs. The cell viability of the highest concentration (200 µg/mL) was 22.47%, indicating the well efficiency of *P. australis*-AuNPs as the anticancer agent (Fig. 6).

Sathishkumar et al. (2015) reported lower efficiencies of phyto (by the extract of star anise (*Illicium verum*) and chemosynthesized AuNPs with an equal concentration (200 µg/mL) against A549 cancer cells.

Antioxidant activity of AuNPs (DPPH assay)

Free radicals cause cell damage and mutations, so they are harmful to human health. On the other side, antioxidant materials nowadays are playing a significant role against any free radicals. The antioxidant agent that proved extreme efficiency is AuNPs, especially those biologically synthesized (Wang et al. 2016). Additionally, DPPH is a well-known technique utilized to assess the antioxidant potency of various antioxidants (Quinten et al. 1985; Majumdar et al. 2016), while the DPPH consists of many stable free radical molecules and is easily reduced by accepting electron or hydrogen from NPs.

Herein, the antioxidant capability of AuNPs was estimated and drawn in Fig. 7. As shown from the results, the AuNPs possessed good quenching for DPPH with a scavenging percentage equals to 10.26%. Moreover, the activity decreased as the AuNPs concentration decreased. The current result demonstrated that the plant originated capping layer contains many compounds as flavonoids, glycosides and phenols, which may add more support to the scavenging potentiality of the phytosynthesized AuNPs. Comparable results were also recorded by Zayed et al. (2020). The achieved antioxidant potency for the AuNPs was mainly due to the existence of polyphenolic compounds in the leaf extract that possess beneficial biological activities, frequently utilized as antioxidants (Mariychuk et al. 2020).

Photocatalytic potential

Figure 8 showed the catalytic efficacy of two different volumes of AuNPs (250 and 500 µL) for MB degradation. The MB has a characteristic peak in the visible region at 664 nm; after the addition of phytoprepared AuNPs, the blue color of MB disappeared after 1 min. This could be attributed to the tiny particle size that induced a large surface area of AuNPs, leading to accelerating the process of electron transfer between $NaBH_4$ and MB and eventually resulting in MB catalytic removal. In particular, the role of AuNPs in the photocatalytic removal of MB serving in the electron

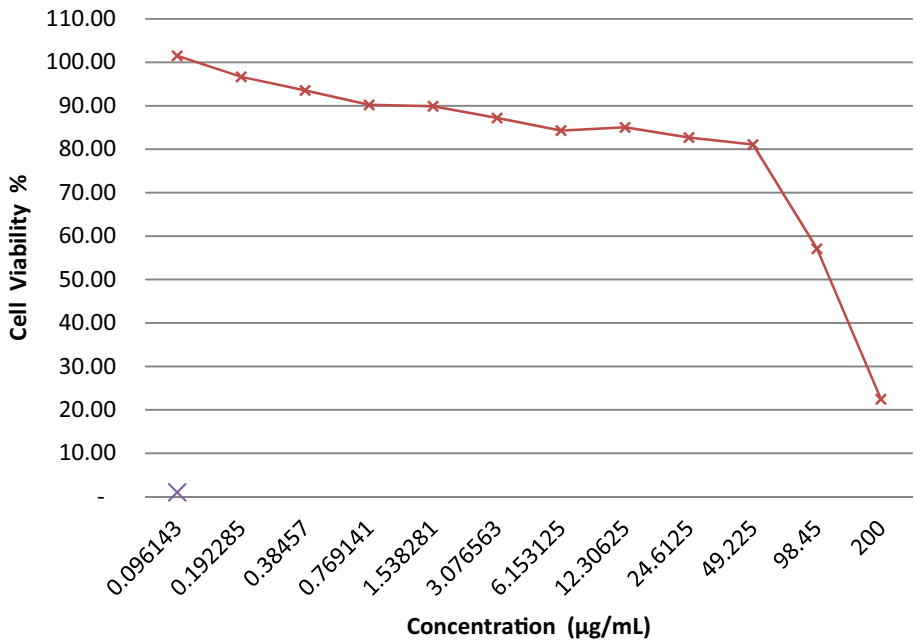

Fig. 6 Cell viability % efficiency of the phytosynthesized AuNPs against cancerous lung cells A549 after 48 h of incubation

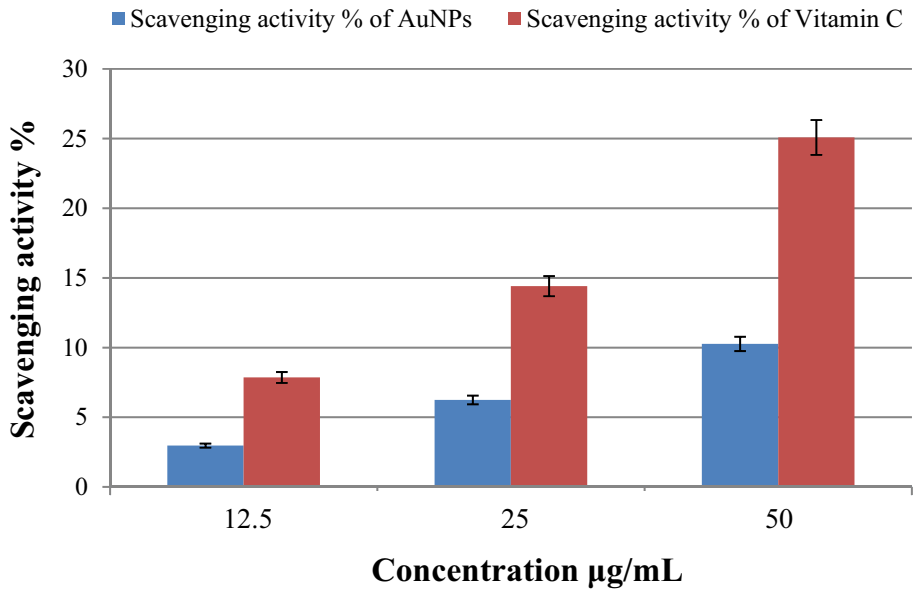

Fig. 7 Free radical scavenging activity of the biosynthesized AuNPs

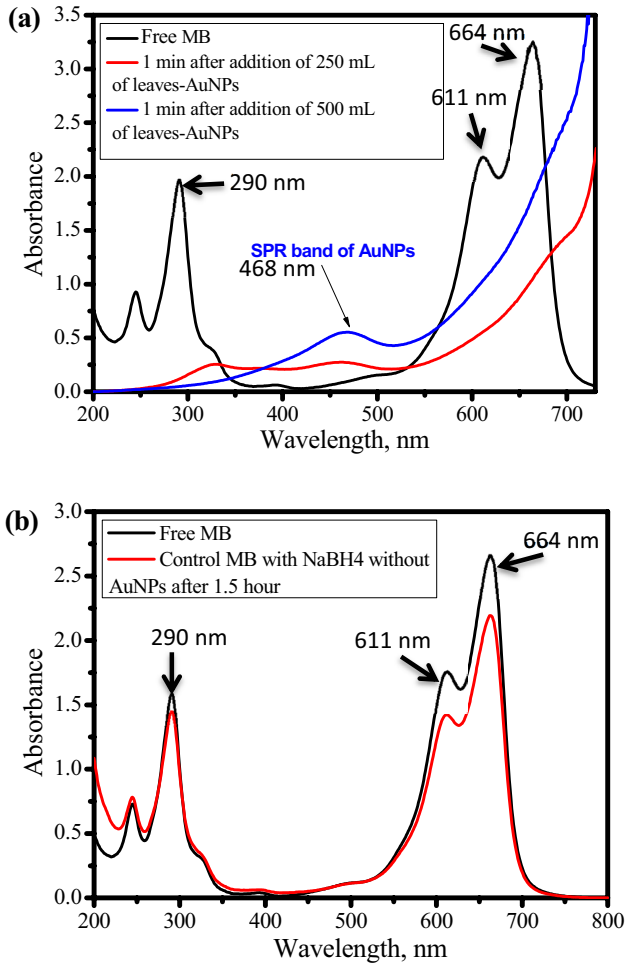

Fig. 8 the photocatalytic potential of AuNPs for degradation of MB, **a** with AuNPs **b** without using AuNPs

transmit from BH_4^- (donor) to MB (acceptor). BH_4^- ions are nucleophilic, while MB is electrophilic in nature with respect to AuNPs, where the AuNPs accept electrons from BH_4^- ions and transports them to the MB. Therefore, this will result in MB removal, as indicated by Ganapuram et al. (2015). On the other hand, the control sample that contains $NaBH_4$ without adding AuNPs showed a removal efficiency of 17.50% after 1 and a half hours. It was thus proving the prominent role of AuNPs in catalyzing the MB removal.

Recently, Ahmad et al. (2020) postulated that MB molecules are successfully degraded in the presence of a visible light source, owing to the efficient oxidation via formation of hydroxyl radicals during photocatalytic removal reaction mechanism. The photogenerated electrons successfully produced hydroxyl radicals as well as superoxide radicals to react with dissolved oxygen. These radicals may insistently attack the MB molecules until a complete removal. The electrostatic attraction forces were also responsible for the adsorption of MB over the surface of AuNPs. Therefore, it could be assumed that the same radicals were responsible for MB removal through degradation or adsorption in the current study.

Conclusions

This work demonstrated common reed leaf extract's ability to synthesize AuNPs by a simple, facile, cheap, and eco-friendly method. UV–Vis spectroscopy, FT-IR, XRD, EDX, Zeta potential, and TEM techniques were utilized to describe the biosynthesized AuNPs. TEM images revealed the formation of several shapes. However the dominant was the spherical with a size around 18 nm. Zeta potential was

– 13.0, while its SPR peak centered at 540 nm. The FT-IR proposed that polyphenolic compounds, e.g., flavonoids containing H–bonded (OH) group, could be liable for the reduction and capping of AuNPs. The XRD and EDX results showed a crystalline Face Center Cubic (FCC) structure. Cytotoxic investigation through MTT assay showed a good cytotoxic effect against A549 cancer cell line. Moreover, the phytosynthesized AuNPs acquired good antioxidant efficiency against DPPH. Furthermore, a high catalytic potential was obtained after 1 min for the removal of MB dye. These findings contribute to the green route of the emerging medical nano-based technologies. Also, provide a new option for the environmental management of the huge unwanted biomass of common reed.

Supplementary Information The online version contains supplementary material available at https://doi.org/10.1007/s13204-021-01776-w.

Acknowledgements This work was financially supported by SMART WATIR, ERANETMED-3-227 project, Egyptian Academy of Scientific Research and Technology and Young Scientist Research Grant 2020. Egyptian National MAB Committee for UNESCO. Egypt Ministry of Higher Education code: IPH1-021-KAF.

Declarations

Conflict of interest There are no conflicts of interest.

References

AbdelHamid AA, Al-Ghobashy MA, Fawzy M, Mohamed MB, Abdel-Mottaleb MM (2013) Phytosynthesis of Au, Ag, and Au–Ag bimetallic nanoparticles using aqueous extract of sago pondweed (*Potamogeton pectinatus* L.). ACS Sustain Chem Eng 1:1520–1529

Abel EE, Poonga PRJ, Panicker SG (2016) Characterization and in vitro studies on anticancer, antioxidant activity against colon cancer cell line of gold nanoparticles capped with *Cassia tora* SM leaf extract. Appl Nanosci 6:121–129

Ahmad T et al (2020) Controllable phytosynthesis of gold nanoparticles and investigation of their size and morphology-dependent photocatalytic activity under visible light. J Photochem Photobiol A. https://doi.org/10.1016/j.jphotochem.2020.112429

Al-Akeel K, Reynolds A, Choudhary A (2010) Phytoremediation of waterways using reed plants

Amendola V et al. (2014) Physico-chemical characteristics of gold nanoparticles. In: Comprehensive analytical chemistry, vol 66. Elsevier, pp 81–152

Arvindganth R, Kathiravan G (2019) Biogenic synthesis of gold nanoparticle from *Enicostema axillare* and their in vitro cytotoxicity study against MCF-7 cell line. Bio Nanosci 9:839–847

Capek I (2017) Nanofield. In: Lockwood DJ (ed) Noble metal nanoparticles. Springer, Tokyo. https://doi.org/10.1007/978-4-431-56556-7_1

Chellapandian C, Ramkumar B, Puja P, Shanmuganathan R, Pugazhendhi A, Kumar P (2019) Gold nanoparticles using red seaweed *Gracilaria verrucosa*: green synthesis, characterization and biocompatibility studies. Process Biochem 80:58–63

Derouiche S, Azzi M, Hamida A (2017) Effect of extracts aqueous of phragmites australis on carbohydrate metabolism, some enzyme activities and pancreatic islet tissue in alloxaninduced diabetic rats. Int J Pharm Pharm Sci 9:54–58

Dubey SP, Lahtinen M, Sillanpää M (2010) Green synthesis and characterizations of silver and gold nanoparticles using leaf extract of *Rosa rugosa*. Colloids Surf A 364:34–41

El-Borady OM, Ayat MS, Shabrawy MA, Millet P (2020) Green synthesis of gold nanoparticles using Parsley leaves extract and their applications as an alternative catalytic, antioxidant, anticancer, and antibacterial agents. Advanc Powder Technol 31:4390–4400

Ganapuram BR, Alle M, Dadigala R, Dasari A, Maragoni V, Guttena V (2015) Catalytic reduction of methylene blue and congo red dyes using green synthesized gold nanoparticles capped by salmalia malabarica gum. Int Nano Lett 5:215–222

Geetha R, Ashokkumar T, Tamilselvan S, Govindaraju K, Sadiq M, Singaravelu G (2013) Green synthesis of gold nanoparticles and their anticancer activity. Cancer Nanotechnol 4:91–98

Hamelian M, Hemmati S, Varmira K, Veisi H (2018a) Green synthesis, antibacterial, antioxidant and cytotoxic effect of gold nanoparticles using Pistacia Atlantica extract. J Taiwan Inst Chem Eng 93:21–30

Hamelian M, Varmira K, Veisi H (2018b) Green synthesis and characterizations of gold nanoparticles using thyme and survey cytotoxic effect, antibacterial and antioxidant potential. J Photochem Photobiol B 184:71–79

He X, Fu L, Yang H (2014) Insight into the nature of Au-Au_2O_3 functionalized palygorskite. Appl Clay Sci 100:118–122

Karmous I, Pandey A, Haj KB, Chaoui A (2019) Efficiency of the green synthesized nanoparticles as new tools in cancer therapy: insights on plant-based bioengineered nanoparticles, biophysical properties, and anticancer roles. Biol Trace Element Res 196:1–13

Kumari P, Meena A (2020) Green synthesis of gold nanoparticles from lawsoniainermis and its catalytic activities following the Langmuir-Hinshelwood mechanism. Colloids Surf A. https://doi.org/10.1016/j.colsurfa.2020.125447

Lee YJ, Ahn E-Y, Park Y (2019) Shape-dependent cytotoxicity and cellular uptake of gold nanoparticles synthesized using green tea extract. Nanoscale Res Lett 14:1–14

Liu Z, Zhao F, Gao S, Shao J, Chang H (2016) The applications of gold nanoparticle-initiated chemiluminescence in biomedical detection. Nanoscale Res Lett 11:1–8

Mafuné F, Kohno J-y, Takeda Y, Kondow T (2002) Full physical preparation of size-selected gold nanoparticles in solution: laser ablation and laser-induced size control. J Phys Chem B 106:7575–7577

Mahendran G, Ponnuchamy K (2018) Coumarin–gold nanoparticle bioconjugates: preparation, antioxidant, and cytotoxic effects against MCF-7 breast cancer cells. Appl Nanosci 8:447–453

Majumdar R, Bag BG, Ghosh P (2016) Mimusops elengi bark extract mediated green synthesis of gold nanoparticles and study of its catalytic activity. Appl Nanosci 6:521–528

Manikandakrishnan M et al (2019) Facile green route synthesis of gold nanoparticles using *Caulerpa racemosa* for biomedical applications. J Drug Deliv Sci Technol. https://doi.org/10.1016/jddst.2019.101345

Manivasagan P, Alam MS, Kang K-H, Kwak M, Kim S-K (2015) Extracellular synthesis of gold bionanoparticles by Nocardiopsis sp. and evaluation of its antimicrobial, antioxidant and cytotoxic activities. Bioprocess Biosyst Eng 38:1167–1177

Mariychuk R, Fejer J, Porubska J, Grishchenko LM, Lisnyak VV (2020) Green synthesis and characterization of gold triangular nanoprisms using extract of *Juniperus communis* L. Appl Nanosci 10:2835–2841

Markus J, Wang D, Kim Y-J, Ahn S, Mathiyalagan R, Wang C, Yang DC (2017) Biosynthesis, characterization, and bioactivities evaluation of silver and gold nanoparticles mediated by the roots of Chinese herbal *Angelica pubescens*. Maxim Nanoscale Res Lett 12:1–12

Mhamane D et al (2011) From graphite oxide to highly water dispersible functionalized graphene by single step plant extract-induced deoxygenation. Green Chem 13:1990–1996

Mikhlin Y, Likhatski M, Tomashevich Y, Romanchenko A, Erenburg S, Trubina S (2010) XAS and XPS examination of the Au–S nanostructures produced via the reduction of aqueous gold (III) by sulfide ions. J Electron Spectros Relat Phenom 177:24–29

Milaneze BA et al (2016) Facile synthesis of monodisperse gold nanocrystals using *Virola oleifera*. Nanoscale Res Lett 11:465

Mohamed M, Adbel-Ghani N, El-Borady O, El-Sayed M (2012) 5-Fluorouracil induces plasmonic coupling in gold nanospheres: new generation of chemotherapeutic agents

Nadagouda MN, Varma RS (2008) Green synthesis of silver and palladium nanoparticles at room temperature using coffee and tea extract. Green Chem 10:859–862

Nakkala JR, Mata R, Bhagat E, Sadras SR (2015) Green synthesis of silver and gold nanoparticles from *Gymnema sylvestre* leaf extract: study of antioxidant and anticancer activities. J Nanopart Res 17:1–15

Narayanan KB, Park HH (2015) Homogeneous catalytic activity of gold nanoparticles synthesized using turnip (*Brassica rapa* L.) leaf extract in the reductive degradation of cationic azo dye. Korean J Chem Eng 32:1273–1277

Neouze M-A (2013) Nanoparticle assemblies: main synthesis pathways and brief overview on some important applications. J Mater Sci 48:7321–7349

Noruzi M, Zare D, Davoodi D (2012) A rapid biosynthesis route for the preparation of gold nanoparticles by aqueous extract of cypress leaves at room temperature. Spectrochim Acta Part A Mol Biomol Spectrosc 94:84–88

Ono LK, Roldan Cuenya B (2008) Formation and thermal stability of Au_2O_3 on gold nanoparticles: size and support effects. J Phys Chem C 112:4676–4686

Parveen A, Rao S (2015) Cytotoxicity and genotoxicity of biosynthesized gold and silver nanoparticles on human cancer cell lines. J Cluster Sci 26:775–788

Paul K, Bag BG, Samanta K (2014) Green coconut (*Cocos nucifera* L.) shell extract mediated size controlled green synthesis of polyshaped gold nanoparticles and its application in catalysis. Appl Nanosci 4:769–775

Princy K, Gopinath A (2018) Optimization of physicochemical parameters in the biofabrication of gold nanoparticles using marine macroalgae *Padina tetrastromatica* and its catalytic efficacy in the degradation of organic dyes. J Nanostruct Chem 8:333–342

Quinten M, Kreibig U, Schönauer D, Genzel L (1985) Optical absorption spectra of pairs of small metal particles. Surf Sci 156:741–750

Rajab M et al (2014) Control of spatial organization of gold nanoparticles using cylindrical nanopores of block copolymers films. Phys Procedia 55:396–402

Ramamurthy C, Padma M, Mareeswaran R, Suyavaran A, Kumar MS, Premkumar K, Thirunavukkarasu C (2013) The extra cellular synthesis of gold and silver nanoparticles and their free radical scavenging and antibacterial properties. Colloids Surf B 102:808–815

Reddy GB, Madhusudhan A, Ramakrishna D, Ayodhya D, Venkatesham M, Veerabhadram G (2015) Green chemistry approach for the synthesis of gold nanoparticles with gum kondagogu: characterization, catalytic and antibacterial activity. J Nanostruct Chem 5:185–193

Sathishkumar M, Pavagadhi S, Mahadevan A, Balasubramanian R (2015) Biosynthesis of gold nanoparticles and related cytotoxicity evaluation using A549 cells. Ecotox Environ Safe 114:232–240

Sedki M, Mohamed MB, Fawzy M, Abdelrehim DA, Abdel-Mottaleb MM (2015) Phytosynthesis of silver–reduced graphene oxide (Ag–RGO) nanocomposite with an enhanced antibacterial effect using *Potamogeton pectinatus* extract. RSC Adv 5:17358–17365

Sett A, Gadewar M, Sharma P, Deka M, Bora U (2016) Green synthesis of gold nanoparticles using aqueous extract of *Dillenia indica*. Adv Nat Sci 7(2):025005

Shaltout K, Al-Sodany Y, Eid E (2006) Biology of common reed Phragmites Australis (cav) trin ex steud: review and inquiry. Assiut University Center for Environmental Studies (AUCES)

Sree Satya Bharati M, Byram C, Soma VR (2018) Femtosecond laser fabricated Ag@ Au and Cu@ Au alloy nanoparticles for surface enhanced Raman spectroscopy based trace explosives detection. Front Phys. https://doi.org/10.3389/fphy.2018.00028

Sun Y, Xia Y (2002) Shape-controlled synthesis of gold and silver nanoparticles. Science 298:2176–2179

Tahar IB, Fickers P, Dziedzic A, Płoch D, Skóra B, Kus-Liśkiewicz M (2019) Green pyomelanin-mediated synthesis of gold nanoparticles: modelling and design, physico-chemical and biological characteristics. Microb Cell Fact 18:1–11

Thangamani N, Bhuvaneshwari N (2019) Green synthesis of gold nanoparticles using Simarouba glauca leaf extract and their biological activity of micro-organism. Chem Phys Lett. https://doi.org/10.1016/j.cplett.2019.07.015

Torabi N, Nowrouzi A, Ahadi A, Vardasbi S, Etesami B (2019) Green synthesis of gold nanoclusters using seed aqueous extract of *Cichorium intybus* L. and their characterization. SN Appl Sci 1:1–14

Torres J, Perry CC, Bransfield SJ, Fairbrother DH (2002) Radical reactions with organic thin films: chemical interaction of atomic oxygen with an X-ray modified self-assembled monolayer. J Phys Chem B 106:6265–6272

Vijayan R, Joseph S, Mathew B (2019) Anticancer, antimicrobial, antioxidant, and catalytic activities of green-synthesized silver and gold nanoparticles using *Bauhinia purpurea* leaf extract. Bioprocess Biosyst Eng 42:305–319

Wang C et al (2016) Characterization and antimicrobial application of biosynthesized gold and silver nanoparticles by using Microbacterium resistens. Artif Cells Nanomed Biotechnol 44:1714–1721

Zayed MF, Mahfoze RA, El-kousy SM, Al-Ashkar EA (2020) In-vitro antioxidant and antimicrobial activities of metal nanoparticles biosynthesized using optimized Pimpinella anisum extract. Colloids Surf A. https://doi.org/10.1016/j.colsurfa.2019.124167